Heterogeneous & Homogeneous & Bio- & Nano-

CHEMCATCHEM

CATALYSIS

Accepted Article

Title: Implanting Copper-Zinc Nanoparticles into the Matrix of Mesoporous Alumina as a Highly Selective Bifunctional Catalyst for Direct Synthesis of Dimethyl Ether from Syngas

Authors: Yingqi Sun and Zhongkui Zhao

To be cited as: *ChemCatChem* 10.1002/cctc.201902166

Link to VoR: http://dx.doi.org/10.1002/cctc.201902166

A Journal of

ChemPubSoc Europe

WILEY-VCH

www.chemcatchem.org

Implanting Copper-Zinc Nanoparticles into the Matrix of Mesoporous Alumina as a Highly Selective Bifunctional Catalyst for Direct Synthesis of Dimethyl Ether from Syngas

Yingqi Sun and Zhongkui Zhao*

Abstract: Dimethyl ether (DME) is an industrially important intermediate and clean alternative fuel. Thus developing an efficient bifunctional catalyst for syngas-to-DME is practically important but remains a challenge. In this paper, a copper-zinc implanting into matrix of mesoporous alumina (CuZn@*m*-Al_2O_3) catalyst was prepared by introducing the as-prepared Cu-Zn oxalate nanoparticles into the $Al(_i\text{-}OPr)_3$-containing precursor solution for preparing mesoporous Al_2O_3 (*m*-Al_2O_3) through evaporation-inducing assembly method. The preparation of Cu-Zn oxalate in advance for synthesizing CuZn@*m*-Al_2O_3 can intensify the Cu-ZnO interaction, confirmed by XRD and H_2-TPR. Thanks to the unique CuZn-implanting closed structure, CuZn@*m*-Al_2O_3 shows 89.0% of higher selectivity with comparable CO conversion (15.5%) than the previously reported supported-type CuZn catalyst on *m*-Al_2O_3 (CuZn/*m*-Al_2O_3, 75.2%) for hydrogenation of syngas to DME. Over the developed CuZn@*m*-Al_2O_3 catalyst, 0.16 mmol g^{-1}_{cat} h^{-1} of high DME rate can be achieved. CuZn@*m*-Al_2O_3 also shows higher methanation resistance (2.7% CH_4) compared to CuZn/*m*-Al_2O_3 (6.3%), ascribed to intensified Cu-Zn interaction owing to the as-formation of Cu-Zn oxalate in advance. Moreover, Both CuZn@*m*-Al_2O_3 and CuZn/*m*-Al_2O_3 exhibit high stability. The outstanding catalytic performance of CuZn@*m*-Al_2O_3 allows it to be a promising catalyst for DME synthesis from syngas.

Nowadays, dimethyl ether (DME) has attracted more and more attention concerning its application acting as both an industrially important chemical materials and a clean alternative fuel.[1-5] DME was generally produced by two routes: one is methanol dehydration catalyzed by an acidic catalyst, in which methanol is previously synthesized by catalyzed hydrogenation of syngas; the other is a direct synthesis route from one-pot transformation of syngas over a bifunctional catalyst.[5-11] The latter is regarded as a promising pathway for DME production. The generally used bifunctional catalyst for the one-step synthesis of DME from syngas is composed of two types of active sites: one is methanol synthesis transition metallic catalyst, and the other is methanol dehydration solid acid catalyst. Regarding methanol synthesis process, Cu-ZnO catalysts have been extensively studied for decades. Traditionally, impregnation, co-precipitation, chemical vapor deposition, sol–gel and other wet-chemical methods have been widely used to prepare Cu-ZnO based catalysts.[11-18] For solid acid catalysts, H-ZSM-5 and γ-Al_2O_3 are generally considered excellent candidates for methanol dehydration to DME and other acidic catalysis processes.[11,14,19,20] Previous studies have paid more attention to the simple mechanical mixing of the two catalysts.[22-27] However, some deficiencies like copper sintering and far distance between active sites of syngas-to-methanol and solid acidic sites cannot be avoided in one-pot transformation process over this kind of mixed hybrid catalyst.[28-32]

Many efforts have been done to overcome the above problems.[33-41] The confinement of Cu-Zn into the pores of high thermal stability mesoporous Al_2O_3 can efficiently enhance the catalytic stability by suppressing the aggregation of Cu nanopartilces,[33-35] but the selectivity of DME remains to be improved owing to the as-formed methanol on the Cu catalyst easily leaving the catalyst through the mesopores before it to be converted into DME by dehydration. In order to address this issue, various core-shell catalysts with Cu-Zn as core and zeolite as shell have been reported.[36-41] Thanks to the confinement effect of core-shell structure, thus catalysts have shown much high DME selectivity since the as-formed methanol must pass through the zeolite shell before it leaves from the catalyst. Unfortunately, the process of coating zeolite shell on the CuZn core inevitably etches the Cu-based core, which would deteriorate the catalytic activity of CuZn@zeolite core-shell although it shows outstanding selectivity of DME. Therefore, pursuing a new and highly efficient Cu-based bifunctional catalyst with high active and selectivity still remains a challenge.

In this work, we design and prepare CnZn embedding-type bifunctional catalyst into the matrix of *m*-Al_2O_3 by adding the as-formed CuZn oxalate into the precursor solution in the preparation process of *m*-Al_2O_3. The developed CuZn@Al_2O_3 catalyst shows much higher selectivity of DME than the previously reported CuZn/*m*-Al_2O_3 catalyst prepared by impregnating CuZn on the *m*-Al_2O_3 support. Moreover, both CuZn@Al_2O_3 and CuZn/*m*-Al_2O_3 catalysts show high activity and stability. The outstanding catalytic performance of CuZn@*m*-Al_2O_3 catalyst allows it to be a promising candidate for direct DME production from syngas. This work not only creates a novel and highly efficient bifunctional syngas-to-DME catalyst, but also presents a new conception for designing highly efficient bifunctional catalysts for other consecutive reactions.

Scheme 1 depicts the schematic illustration for the preparation of the developed CuZn@*m*-Al_2O_3 bifunctional catalyst. Typically, the CuZn@*m*-Al_2O_3 catalyst was prepared by the following 4 steps: (1) The CuZn oxalate was prepared by co-precipitation method with oxalic acid as precipitant as well as the $Cu(NO_3)_2$ and $Zn(NO_3)_2$ as Cu and Zn precursors, respectively; (2) Pluronic P123, aluminum isopropoxide and HNO_3 were dissolved in ethanol solvent under strong stirring at ambient temperature for 6 hours to form precursor solution of *m*-Al_2O_3; (3) The CuZn oxalate powder were added to the above precursor solution; (4) The solvent was evaporated and then transferred to an drying oven, and finally calcined at 400 °C and

[a] Yingqi Sun, and Prof. Zhongkui Zhao
State Key Laboratory of Fine Chemicals Department of Catalysis Chemistry and Engineering School of Chemical Engineering Dalian University of Technology Dalian 116024, P.R. China
E-mail: zkzhao@dlut.edu.cn

Supporting information for this article is given via a link at the end of the document.((Please delete this text if not appropriate))

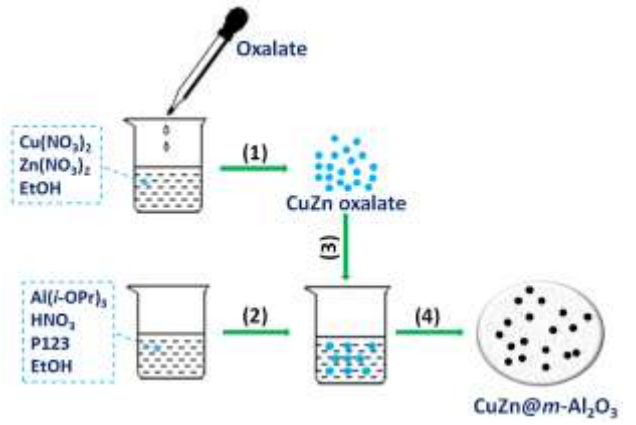

Scheme 1. Schematic illustration of the preparation of implanting-type CuZn@*m*-Al_2O_3 bifunctional catalyst.

then 600 °C for oxalate decomposition and mesoporous Al_2O_3 formation. As a consequence, the implanting-type CuZn@*m*-Al_2O_3 was prepared. Moreover, the supporting-type CuZn/*m*-Al_2O_3 was prepared by incipient wetness impregnation method for comparison.

Figure 1 shows TEM images of as-synthesized CuZn@*m*-Al_2O_3 and CuZn/*m*-Al_2O_3. From Figure 1, CuZn nanoparticles

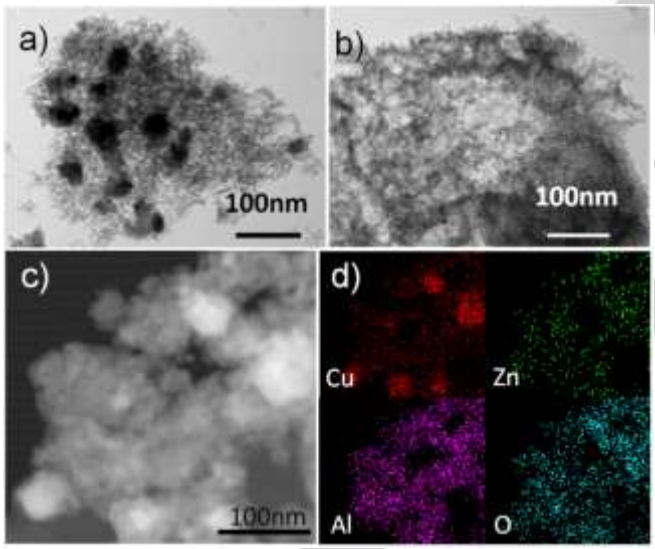

Figure 1. a,b) TEM images of CuZn@*m*-Al_2O_3 (a) and CuZn/*m*-Al_2O_3 (b). c,d) STEM image (c) and the corresponding mapping image (d) of CuZn@*m*-Al_2O_3 catalyst.

with the size of 30-60 nm are implanted into the matrix of CuZn@*m*-Al_2O_3 while the smaller CuZn dispersed into the *m*-Al_2O_3 of CuZn/*m*-Al_2O_3 catalyst. The bigger CuZn size in the CuZn@*m*-Al_2O_3 catalyst than that of CuZn/*m*-Al_2O_3 leads to its lower surface area of exposed Cu (8.35 vs. 9.59 m^2 g^{-1}.). Furthermore, the unique implanting-type CuZn@*m*-Al_2O_3 catalyst featuring the CuZn nanoparticles to be embedded into the matrix of *m*-Al_2O_3 is confirmed by the STEM and the corresponding mapping images (Figure 1c and 1d). The textural properties of the two catalysts were characterized by N_2 adsorption-desorption experiments, and the bare *m*-Al_2O_3 is also included for comparison. **Figure 2** shows the isotherms and

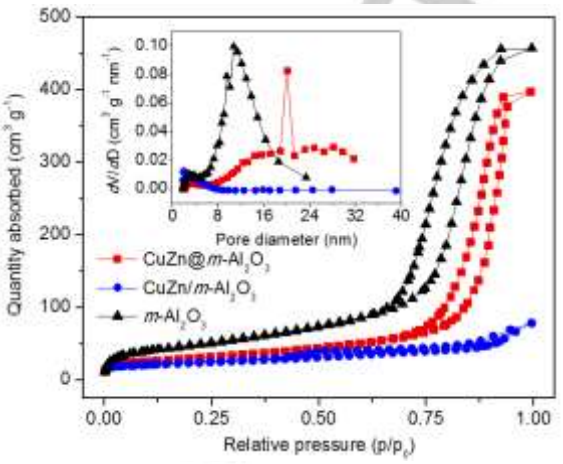

Figure 2. Nitrogen adsorption-desorption isotherms of *m*-Al_2O_3, CuZn@*m*-Al_2O_3 and CuZn/*m*-Al_2O_3. Inset: pore size distributions from adsorption branch

the pore size distribution regarding mesopores, and the quantitative data are listed in **Table 1**. The mesoporous

Table 1. Characterization data of the CuZn@*m*-Al_2O_3 , CuZn/*m*-Al_2O_3 and *m*-Al_2O_3 catalysts.

Catalyst	S_{BET}[a] [m^2 g^{-1}]	V_P[b] [cm^3 g^{-1}]	D_P[c] [nm]	S_{Cu}[d] [m^2 g^{-1}_{cat}]
CuZn@*m*-Al_2O_3	108	0.62	14.9	8.35
CuZn/*m*-Al_2O_3	55	0.11	6.0	9.59
m-Al_2O_3	201	0.72	9.5	

[a] BET specific surface area from N_2 adsorption desorption. [b] Total pore volume (cm^3 g^{-1}). [c] Average pore diameter (nm). [d] Surface area of Cu were determined from by H_2-TPR after oxidation of the samples by N_2O.

structures of the solid acid *m*-Al_2O_3 and CuZn@*m*-Al_2O_3 catalysts were confirmed by the typical type IV adsorption–desorption isotherms.[33] However, the typical type IV adsorption-desorption isotherm cannot be observed on the CuZn/*m*-Al_2O_3 catalyst although the *m*-Al_2O_3 support has a typical ssmesoporous structure, might be ascribed to the blockage of mesopores of *m*-Al_2O_3 by a large amount of CuZn nanoparticles. Moreover, the CuZn@*m*-Al_2O_3 catalyst shows higher surface area (108 m^2 g^{-1}) and mesoporous volume (0.62 cm^3 g^{-1}) compared to CuZn/Al_2O_3 catalyst (55 m^2 g^{-1}, 0.11 cm^3 g^{-1}).

To acquire the crystalline structure of these materials, this work used X-ray diffraction (XRD) to obtain the result. As isshown in **Figure 3**, the characteristic diffractions peaks of CuO are located at 35.6, 38.8, 58.3, 61.6, and 66.3° and the XRD peaks at 34.2 and 48.1° corresponding to ZnO phase can be resolved [40-42]. Furthermore, the characteristic X-ray diffraction peaks at 66.1° corresponding to *m*-Al_2O_3 of the CuZn@*m*-Al_2O_3 samples can be resolved, presenting an evidence for the

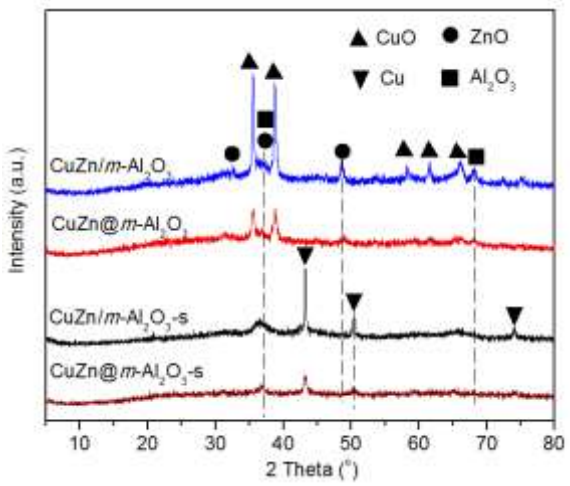

Figure 3. XRD patterns of *m*-CuZn@Al_2O_3, CuZn/*m*-Al_2O_3, CuZn@*m*-Al_2O_3-s, and CuZn/*m*-Al_2O_3-s.

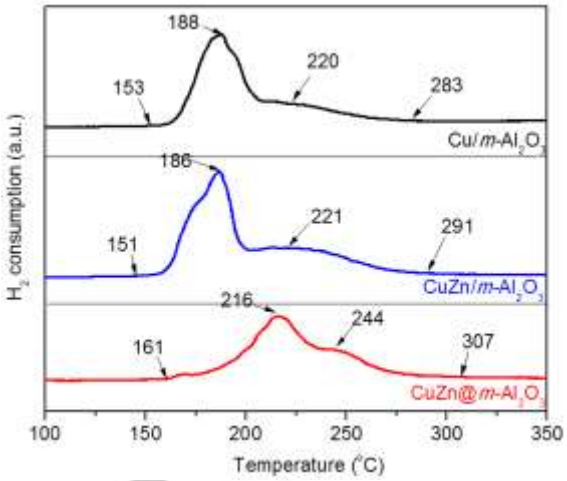

Figure 4. H_2-TPR profiles of the CuZn@*m*-Al_2O_3 and CuZn/*m*-Al_2O_3 catalysts, and the Cu/*m*-Al_2O_3 is included for comparison.

successful coating *m*-Al_2O_3. Moreover, CuZn@*m*-Al_2O_3 shows obviously weaker and wider diffraction peaks assigned to CuO and ZnO compared to those of CuZn/*m*-Al_2O_3, suggesting smaller crystalline size of CuO and ZnO. The average crystalline size of CuO was estimated by Scherrer Equation (Table S1), CuZn@*m*-Al_2O_3 catalyst shows lower CuO average crystalline size (29.7 nm) compared CuZn/*m*-Al_2O_3 (41.6 nm), although the former shows larger particle size confirmed by TEM images shown in Figure 1. After reduction, the CuO can be transformed into metallic Cu. The smaller crystalline size of Cu and ZnO leads to the intensified Cu-ZnO interaction. According to the reference,[5] ZnO can maintain high copper dispersion through Cu-ZnO interaction in CuZn@*m*-Al_2O_3 catalyst, which can promote methanol synthesis and inhibit methane formation. The ZnO peaks after the reaction of the two catalysts all shifted to the right, indicates that the crystal structure of the ZnO changed after the reaction.

The H_2-TPR was carried out to investigate the redox behavior and the interaction of Cu particles with Zn species of the *m*-CuZn/Al_2O_3 and CuZn@*m*-Al_2O_3 catalysts, and Cu/m-Al_2O_3 was included for comparison. From **Figure 4**, the reference supported single Cu catalyst on *m*-Al_2O_3 exhibits two H_2-consumption peaks appearing at 188 and 220 °C, corresponding to the reduction of highly dispersed CuO in copper-zinc oxide and the reduction of bulk CuO crystals with larger grain sizes dispersed among ZnO particles, respectively. Compared with Cu/*m*-Al_2O_3, the CuZn/*m*-Al_2O_3 shows similar reduction peaks, but the reduction peak at high temperature becomes more obvious. Furthermore, the reduction peaks of CuZn@*m*-Al_2O_3 shift to higher reduction temperature compared to those of CuZn/*m*-Al_2O_3, might be ascribed to unique structure featuring the CuZn nanoparticles implanted into the matrix of m-Al_2O_3, besides the intensified Cu-ZnO interaction.[26] According to Table S1, the H_2 consumption of CuZn@*m*-Al_2O_3 (24.2 mmol g^{-1}) is lower than that of CuZn/*m*-Al_2O_3, which might be an indicator for the embedding Cu-Zn into the matrix of *m*-Al_2O_3.

The acidic properties of the as-prepared CuZn@*m*-Al_2O_3 and CuZn/*m*-Al_2O_3 bifunctional catalysts were measured by NH_3-TPD technique, and the spent catalysts (CuZn@*m*-Al_2O_3-s and CuZn/*m*-Al_2O_3-s) were also included for comparison. **Figure 5** presents the NH3-TPD profiles, and the quantitative results are

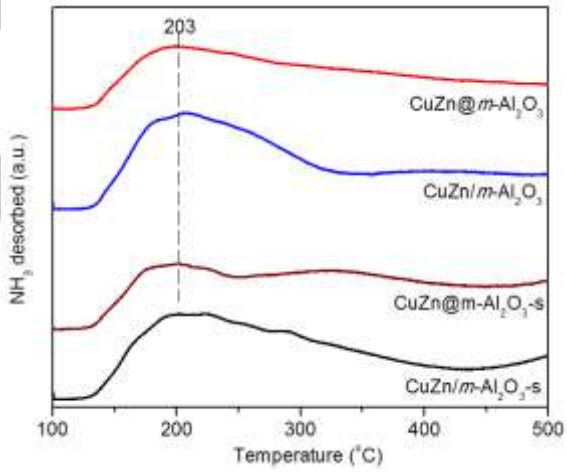

Figure 5. NH_3-TPD profiles of the CuZn@*m*-Al_2O_3, CuZn/*m*-Al_2O_3, CuZn@*m*-Al_2O_3-s and CuZn/*m*-Al_2O_3-s.

listed in Table S1. From Figure 5, all of the samples show a strong peak according to weak acid sites with a broadened peak concerning medium-strength acid sites. Moreover, both of the spent catalysts show a slightly decreasing amount of acidic sites compared to that of the two fresh catalysts, ascribed to the dehydration of surface hydroxyl groups in the reaction process.

The catalytic performance of CuZn@*m*-Al_2O_3 and CuZn/*m*-Al_2O_3 is presented in **Table 2** and S1. The CuZn@*m*-Al_2O_3 catalyst shows slightly higher TOF than CuZn/*m*-Al_2O_3 for direct synthesis of DME from syngas, ascribed to the stronger promotion of ZnO by the intensified Cu-ZnO interaction.[33]

Table 2. Catalytic performance of the CuZn@*m*-Al_2O_3 and CuZn/*m*-Al_2O_3 catalysts for direct synthesis of dimethyl ether from syngas.[a]

catalyst	Con. (%)	CO-to-CO_2 (%)	product distribution[b] (mol %)			TOF (min^{-1})
			MeOH	DME	CH_4	
CuZn/*m*-Al_2O_3	17.4	2.1	18.2	75.2	6.3	1.74
CuZn@*m*-Al_2O_3	15.5	3.2	7.9	89	3.1	1.78
Cu@*m*-Al_2O_3	13.2	2.9	8.6	87.2	4.2	-
Zn@*m*-Al_2O_3	0.8	-	22.5	48.5	29.0	-
CuZnAl[c]	24.7	0.8	93.4	5.1	1.4	-

[a] Reaction condition: 0.5 g catalyst, *P* = 3.0 MPa, *T* = 250 °C, $H_2/CO_2/N_2$ = 10/5/5, *GHSV* = 1800 ml g^{-1} h^{-1}, obtained at 4 h of *TOS*. [b] Based on the as-formed total hydrocarbons and oxygenates. [c] Standard methanol synthesis catalyst.[43]

Interestingly, CuZn@*m*-Al_2O_3 catalyst shows much higher DME distribution (selectivity) with promoted dehydration of methanol to DME than the traditional supported-type CuZn/*m*-Al_2O_3 catalyst although the former shows much more acidic sites (Figure 5), which can be ascribed to the unique implanting-type structure of the developed CuZn@*m*-Al_2O_3 catalyst. In comparison with the standard CuZnAl methanol synthesis catalyst (93.4% methanol selectivity),[43] our CuZn@*m*-Al_2O_3 catalyst can efficiently convert the as-formed methanol from syngas over the implanted CuZn nanoparticles in the matrix of *m*-Al_2O_3 into DME while it passes through the *m*-Al_2O_3. This can be ascribed to the unique implanting-type structure of CuZn@*m*-Al_2O_3 catalyst and the higher Al content (60% vs. 10%). Moreover, CuZn@*m*-Al_2O_3 catalyst shows lower methane content than CuZn/*m*-Al_2O_3 catalyst, originating from the suppressed formation of methane [33] or the promoted conversion of the as-formed methane to methanol[5] by intensified Cu-ZnO interaction. For another, we compared the catalytic performance of the implanted single component catalysts (Cu@*m*-Al_2O_3 and Zn@*m*-Al_2O_3) to present a further insight. From the results listed in Table 2, the addition of Zn shows a promoting effect on the catalytic performance of the supported Cu catalyst in some degree, although only 0.8% conversion over Zn@m-Al_2O_3 can be seen. From XRD and TPR, there is no evidence for the formation of Cu-Zn alloy. From our previous work concerning the CuZnAl prepared by the same method,[40] the Cu-ZnO interaction promotes the catalysis of Cu-based catalyst. Therefore, we proposed that the Cu is the active sites for CO hydrogenation to methanol, and the promoting effect of added Zn into the implanted Cu catalyst in this work might come from the Cu-ZnO interaction at the interface. Furthermore, CuZn@*m*-Al_2O_3 catalyst shows slight higher DME formation rate (0.16 μmol m^{-2}_{Cu} h^{-1}) than the traditional CuZn/*m*-Al_2O_3 catalyst (0.15 μmol m^{-2}_{Cu} h^{-1}).

The catalytic stability of the bifunctional catalysts of two different structures is shown in **Figure 6**. Both of these catalysts show outstanding catalytic stability, and no visible decrease in CO conversion can be observed along with the extending time on stream, although there is a slight decrease in selectivity. By

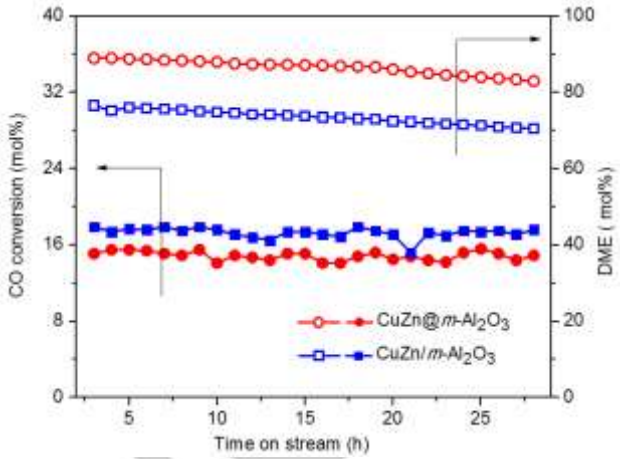

Figure 6. Catalytic stability of CuZn@Al_2O_3 and CuZn/Al_2O_3 for direct synthesis of dimethyl ether from syngas.

comparing the product distributions of the initial and last points listed in Table S2 (TOS = 4 and 28 h), the decreased selectivity mainly comes from the greater amount of methanol (7.9 vs. 13%). The no obvious increase in CH4 can be observed (3.1% vs 3.9%). The slight decrease in DME selectivity can be ascribed to the lowering amount of acidic sites in the reaction process confirmed by the NH_3-TPD profiles presented in Figure 5. In a word, this work develops an efficient bifunctional catalyst for direct synthesis of DME from syngas.

In summary, we report a practical CuZn implanted-type catalyst in the matrix of mesoporous Al_2O_3 simply prepared by addition of the as-prepared CuZn oxalate nanoparticles into the precursor solution according to the preparation of *m*-Al_2O_3. This produces a superior bifunctional catalyst for one-pot DME synthesis from syngas with higher selectivity towards DME from the as-formed methanol over Cu-ZnO to the previously reported supported CuZn catalyst on *m*-Al_2O_3, resulting from its unique implanting-type structure. The prior formation of Cu-Zn oxalate for the preparation of CuZn@*m*-Al_2O_3 catalyst can intensify the Cu-ZnO interaction, which can subsequently stabilize the Cu and also suppress the formation of methane. As a result, the developed CuZn@*m*-Al_2O_3 catalyst shows 15.5% of CO conversion with 89% DME content. This work not only presents highly selective bifunctional catalyst for syngas-to-DME, but also opens up a simple method for designing other bifunctional catalysts for diverse consecutive reactions.

Experimental Section

Catalysts preparation: CuZn@*m*-Al_2O_3 catalyst was prepared by the following procedure: Firstly, binary metal CuZn oxalate particles were prepared by co-precipitation method using oxalate as precipitant. Typically, 1.8 g of oxalic acid in ethanol was added rapidly to a mixed ethanol solution consisting of 1.09 g of copper nitrates and 0.59 g of zinc nitrates in the desired ratio at room temperature under vigorous stirring. The gel-like precipitate was aged for 4 h at room temperature and then separated by centrifugation. The drying process was carried out at 105 °C for 6 h. The obtained CuZn catalyst is crushed into a powder before subsequent use. After that, 2 g of Pluronic P123 was dissolved in 40 mL

of ethanol at room temperature. Then, 2 mL of 67 wt % nitric acid and 4.8 g of aluminum iso-propoxide were added into the above solution with vigorous stirring. The mixture was covered with PE film, stirred at room temperature for about 5 h, and then the as-formed CuZn powder was added into the above solution, and then put into a 60 °C water bath to undergo the solvent evaporation crystallization for 24 h. After aging for 1 day, the as-prepared light blue powder was calcined, the temperature was slowly raised from room temperature to 400 °C (2 °C min^{-1} heating rate) and heated at 400 °C for 4 h. The high temperature treatment was carried out in air at a ramp rate of 10 °C min^{-1} at 600 °C for 2 h. Finally, the CuZn@*m*-Al_2O_3 catalyst was obtained. For comparison, the CuZn/*m*-Al_2O_3 (Cu/*m*-Al_2O_3) catalyst was prepared by loading the same amount of CuZn (Cu) with incipient wetness impregnation method on the *m*-Al_2O_3 support that prepared by the similar method to that for CuZn@*m*-Al_2O_3 catalyst except for no CuZn was introduced.

Catalysts characterization: JEM-2000EX TEM instrument was used to obtain the Transmission electron microscopy (TEM) images. X-ray diffraction (XRD) patterns of the samples were collected in the 2θ range of 5–80° with a step of 0.02° on a Rigaku D/max-2400 apparatus with Cu Kα radiation. NH_3 temperature-programmed desorption (NH_3-TPD) data were acquired on a Builder Chemisorption (PCA-1200) instrument with a thermal conductivity detector (TCD) to measure the desorbed NH_3. The catalyst sample with the amount of 0.1 g was firstly pretreated in flowing argon at 500 °C for 1 h, and then cooled to room temperature. The pretreated sample was saturated with ammonia at 100 °C via pulse injection of ammonia. Desorption profiles were obtained with the flowing argon from 100 °C to 500 °C at a heating rate of 10 °C min^{-1}. Nitrogen adsorption-desorption analysis was applied to measure Brunauer−Emmett−Teller (BET) surface area, pore volume, and Barrett−Joyner−Halenda (BJH) pore size distribution from the desorption branch on the as-prepared Al_2O_3 supports and bifunctional CuZn@Al_2O_3 and CuZn/Al_2O_3 catalysts using a Beishide apparatus Model 3H-2000PS1 at -196 °C. H_2-TPR experiments were performed on a Builder PCA-1200 automated system. 0.03 g of catalyst was placed in a U-shape quartz tube in a temperature‐controlled oven. The catalyst was first purged under Ar flow at 250 °C for 60 min (using a heating rate of 10 °C min^{-1}) and then cooled down to room temperature. After that, it was reduced with a 10% H_2 ‐ 90% Ar mixture (50 mL min^{-1}) by heating to 400 °C at a heating rate of 2 °C min^{-1}. The amount of hydrogen consumption was measured using a thermal conductivity detector. Cu surface areas of samples were determined by H_2-TPR after oxidation of the samples by N_2O at 50 °C. The procedure was as follows: the catalyst sample with the amount of 0.1 g was reduced under 10 % H_2/Ar (30 ml min^{-1}) at 250 °C for 2 h, and then cooled down to room temperature. After purging with He for 30 minutes to remove excess H_2/Ar, the 10% N_2O/He was passed through the sample to oxidize metallic copper at 50 °C for 1 hour. Finally, 10% H_2 /Ar (30 ml min^{-1}) was passed through the sample and the sample temperature was raised to 400 °C at a heating rate of 10 °C min^{-1}. The H_2 consumption is obtained by integrating and converting the TPR peak area. The number of surface area copper atom is twice the number of H_2 molecules consumed. The surface area of the exposed surafce Cu per gram catalyst (S_{Cu}) was calculated by atopting the Eq. 1:

$$S_{Cu} = \frac{n_{Cu} N_A}{C_M W_{cat}} \quad \text{(Eq. 1)}$$

Where n_{Cu} is the number of moles of surface Cu atom calculated by TPR experiment. N_A is the Avogadro constant, C_M is the mean number of copper atoms per m^2 (= 1.46 x 10^{19} m^{-2}),[40] and W_{cat} is the catalyst weight.

Catalytic performance measurement: DME synthesis reaction was performed in a fixed-bed stain-less steel reactor at 250 °C and a total pressure of 3.0 MPa ($CO/N_2/H_2$= 5/5/10) by loading 0.5 g of catalyst (20–40 mesh). The feed flow rate was set at 1800 ml h^{-1} g^{-1}. The prior reduction was performed in situ at 250 °C by a mixture gas (10 ml min^{-1} hydrogen with 20 ml min^{-1} nitrogen) at atmospheric pressure for 2 h. The effluent products from the reactor were transported to the gas chromatography (FULI 9790 II) with tubing warm 160 °C. The GC was equipped with Porapak N and 5A molecular sieve packed columns, which were used to separate inorganic (N_2, CO, CO_2) and organic (CH_4, CH_3OCH_3, CH_3OH) gaseous species, respectively. The CO conversion (X_{CO}) and organic product distribution were calculated using an internal standard method via Eq. 2 and 3, respectively:

$$\text{CO conversion (mol\%)} = \left(1 - \frac{CO_{out}}{CO_{in}}\right) \times 100\ \% \quad \text{(Eq. 2)}$$

$$C^i \text{ distribution (mol\%)} = \frac{\text{Mole of } C^i \times i}{\sum_{i=1}^{n} \text{Mole of } C^i \times i} \times 100\ \% \quad \text{(Eq. 3)}$$

Where CO_{in} and CO_{out} stands for the molar fraction of CO at the inlet and outlet, respectively. C^i represents the organic product of CH_3OH, CH_4, DME, and i is for the carbon number in the molecules.

The formation of CO_2 via the water–gas shift reaction of CO was evaluated by the conversion of CO to CO_2 (mol%). Furthermore, the turnover frequency (TOF) of CO was calcu-lated as the transferred CO per min per surface Cu atom. The intrinsic activity was calculated as the number of moles of as-formed DME per h per m^2 surface area of the exposed Cu atoms. TOF and intrinsic activity were calculated by employing equations 4 and 5, respectively:

$$\text{TOF } \left(min^{-1}\right) = \frac{F_{co} \times X_{co}}{1000 \times V_m \times n_{Cu}} \quad \text{(Eq. 4)}$$

$$\text{Intrinsic activity } R_{DME} = \frac{n_{DME} \times M_{DME}}{S_{Cu} W_{cat}} \quad \text{(Eq. 5)}$$

V_m is the molar volume of an ideal gas at 298 K (24.5 L mol^{-1}), F_{CO} represents the CO flow rate (ml min^{-1}), n_{Cu} is the number of moles of exposed Cu atom of the loaded catalyst for the performance test, M_{DME} is the molecular mass of DME, n_{DME} represents the as-formed DME per min, S_{Cu} is the Cu surface area of samples, and W_{cat} is the mass of catalyst. DME productivity is defined as the number of moles of as-formed DME per h per g catalyst.

Acknowledgements

This work was financially supported by the National Natural Science Foundation of China (U1610104).

Keywords: Cu-Zn catalyst • implantation • syngas • dimethyl ether • bifunctional catalyst • Cu-ZnO interaction

[1] Q. Xie, P. Chen, P. Peng, S. Liu, P. Peng, B. Zhang, Y. Cheng, Y. Wan, Y. Liu, R. Ruan, *RSC Adv*. **2015**, *5*, 26301-26307.
[2] R. Khoshbin, M. Haghighi, *Catal. Sci. Technol*. **2014**, *4*, 1779-1792.
[3] M. Cai, A. Palcic, V. Subramanian, S. Moldovan, O. Ersen, V. Valtchev, V. V. Ordomsky, A. Y. Khodakov, *J. Catal*. **2016**, *338*, 227-238.
[4] A. Bayat, T. Dogu, *Ind. Eng. Chem. Res*. **2016**, *55*, 11431-11439.
[5] A. A. Reule, N. Semagina, *ACS Catal.* **2016**, *6*, 4972-4975.
[6] S. Y. Park, C. H. Shin, J. W. Bae, *Catal. Commun.* **2016**, *75*, 28-31.
[7] Y. D. Chen, Y. Yang, S. L. Tian, Z. Ye, Q. Tang, L. Ye, G. Li, *Appl. Catal. A: Gen.* **2019**, *587*, 117-275.
[8] Z. Cao, T. Hu, J. Guo, J. Xie, N. Zhang, J. Zheng, L. Che, B. H. Chen, *Fuel* **2019**, *254*, 115-524.
[9] Y. Zhang, D. Li, Y. Zhang, Y. Cao, S. Zhang, K. Wang, F. Ding, J. Wu, *Catal. Commun.* **2014**, *55*, 11-15.

[10] Y. J. Lee, M. H. Jung, J. B. Lee, K. E. Jeong, H. S. Roh, Y. W.Suh, J. W. Bae, *Catal. Today* **2014**, *228*, 175-182.
[11] V. V. Ordomsky, M. Cai, V. Sushkevich, S. Moldovan, O. Ersen, C. Lancelot, V. Valtchev, A. Y. Khodakov, *Appl. Catal. A: Gen.* **2014**, *486*, 266-275.
[12] M. Gentzen, W. Habicht, D. E. Doronkin, J. D. Grunwaldt, J. Sauer, S. Behrens, *Catal. Sci. Technol.* **2016**, *6*, 1054-1063.
[13] R. J. Silva, A. F. Pimentel, R. S. Monteiro, C. J. Moto, *J. CO_2 Util.* **2016**, *15* , 83-88.
[14] T. Kaoru, Y. Wagatsuma, H. Ariga, K. Kon, K. Shimizu, *ACS Sustain. Chem. Eng.* **2017**, *5*, 3675-3680.
[15] J. Sun, G. Yang, Q. Ma, I. Ooki, A. Taguchi, T. Abe, Q. Xie, Y. Yoneyama, N. Tsubaki, *J. Mater. Chem. A,* **2014**, *2*, 8637-8643.
[16] Y. Chen, S. Choi, L. T. Thompson, *ACS Catal*. **2015**, *5*, 1717-1725.
[17] H. Li, Z. Su, S. Hu, Y. Yan, *Appl. Catal. B: Environ.* **2017**, *207*, 134-142.
[18] S. Kattel, P. Liu, J. G. Chen, *J. Am. Chem. Soc.* **2017**, *139*, 9739-9745.
[19] C. L. Chiang, K. S. Lin, *Int. J. Hydrogen Energy* **2017**, *42*, 23526-23538.
[20] E. Catizzone, S. V. Daele, M. Bianco, A. D. Michele, A. Aloise, M. Migliori, V. Valtchev, G. Giordano, *Appl. Catal. B: Environ.* **2019**, *243*, 273-282.
[21] S. Y. Cheng, J. W. Kou, Z. H. Gao, W. Huang, *Appl. Catal. A: Gen.* **2018**, *556*, 113-120.
[22] F. Frusteri, M. Cordaro, C. Cannilla, G. Bonura, *Appl. Catal. B: Environ.* **2015**, *162,* 57-65.
[23] G. Bonura, C. Cannilla, L. Frusteri, F. Frusteri, *Appl. Catal. A: Gen.* **2017**, *544*, 21-29.
[24] M. Cai, V. Subramanian, V. V. Sushkevich, V. V. Ordomsky, A. Y. Khodakov, *Appl. Catal. A: Gen.* **2015**, *502*, 370-379.
[25] O. Lupan, V. Cretu, V. Postica, O. Polonskyi, N. Ababii, F. Schutt, V. Kaidas, F. Faupel, R. Adelung, *Sens. Actuators B* **2016**, *230*, 832-843.
[26] A. Garcia-Trenco, E. R. White, M. S. P. Shaffer, C. K. Williams, *Catal. Sci. Technol.* **2016**, *6*, 4389-4397.
[27] F. Frusteri, G. Bonura, C. Cannilla, G. Drago-Ferrante, A. Aloise, E. Catizzone, M. Migliori, G. Giordano, *Appl. Catal. B: Environ.* **2015**, *176-177*, 522-531.
[28] W. Ding, M. Klumpp, H. Li, U. Schygulla, P. Pfeifer, W. Schwieger, K. Haas-Santo, R. Dittmeyer, *J. Phys. Chem. C* **2015**, *119*, 23478-23485.
[29] X. Zhou, T. Su, Y. Jiang, Z. Qin, H. Ji, Z. Guo, *Chem. Eng. Sci.* **2016**, *153*, 10-20.
[30] G. Bonura, M. Migliori, L. Frusteri, C. Cannilla, E. Catizzone, G. Giordano, F. Frusteri, *J. CO_2 Util.* **2018**, *24*, 398-406.
[31] S. Asthana, C. Samanta, R. K. Voolapalli, B. Saha, *J. Mater. Chem. A* **2017,** *5*, 2649-2633.
[32] A. G. Trenco, A. Martinez, *Appl. Catal. A: Gen.* **2012**, *411-412*, 170-179.
[33] H. Ham, J. Kim, S. J. Cho, J. H. Choi, D. J. Moon, J. W. Bae, *ACS Catal*. **2016**, *6*, 5629-5640.
[34] H. Ham, S. W. Baek, C. H. Shin, J. W. Bae, *ACS Catal.* **2019**, *9*, 679-690.
[35] Q. Yuan, A. X. Yin, C. Lou, L. D. Sun, Y. W. Zhang, W. T. Duan, H. C. Liu, C. H. Yan, *J. Am. Chem. Soc.* **2008**, *130*, 3465-3472.
[36] M. Sanchez-Contador, A. Ateka, M. Ibanez, J. Bilbao, A. T. Aguayo, *Renewable Energy* **2019**, *138*, 585-597.
[37] G. Yang, N. Tsubaki, J. Shamoto, Y. Yoneyama, Y. Zhang, *J. Am. Chem. Soc.* **2010**, *132*, 8129-8136.
[38] M. Sanchez-Contador, A. Ateka, A. T. Aguayo, J. Bilbao, *Fuel Process. Technol.* **2018**, *179*, 258-268.
[39] R. Phienluphon, K. Pinkaew, G. Yang, J. Li, Q. Wei, Y. Yoneyama, T. Vitidsant, N. Tsubaki, *Chem. Eng. J.* **2015**, *270*, 605-611.
[40] Y. Sun, X. Hua, Z. Zhao, *Catal. Sci. Technol.* **2019**, *9*, 3763-3770.
[41] W. Ding, M. Klumpp, S. Lee, S. Reuß, S. A. Al-Thabaiti, P. Pfeifer, W. Schwieger, R. Dittmeyer, *Chem. Ind. Technol.* **2015**, *87*, 702-712.
[42] I. Sierra, J. Erena, A. T. Aguayo, J. M. Arandes, M. Olazar, J. Bilbao, *Appl. Catal. B: Environ*. **2011**, *106*, 167-173.
[43] O. Martin, C. Mondelli, D. Curulla-Ferré, C. Drouilly, R. Hauert, J. Pérez-Ramírez, *ACS Catal*. **2015**, *5*, 5607−5616.

Entry for the Table of Contents (Please choose one layout)

Layout 1:

COMMUNICATION

Implanting-type bifunctional catalyst: This work reports a practical CuZn implanted-type catalyst in the matrix of mesoporous Al_2O_3 .This produces a superior bifunctional catalyst for one-pot DME synthesis from syngas with higher selectivity towards DME from the as-formed methanol over Cu-ZnO sites to the previously reported supported CuZn catalyst on *m*-Al_2O_3, resulting from its unique implanting-type structure.

*Yingqi Sun and Zhongkui Zhao**

Page No. – Page No.

Implanting Copper-Zinc Nanoparticles into the Matrix of Mesoporous Alumina as a Highly Selective Bifunctional Catalyst for Direct Synthesis of Dimethyl Ether from Syngas